Contract No:

This document was prepared in conjunction with work accomplished under Contract No. DE-AC09-08SR22470 with the U.S. Department of Energy.

Modeling of $2LiBH_4$+MgH_2 Hydrogen Storage System Accident Scenarios Using Empirical and Theoretical Thermodynamics

C.W. James Jr., D. Tamburello, K. Brinkman,
J.R. Gray, B. Hardy, & D.L. Anton,*

Savannah River National Laboratory
Aiken, SC, 29808 USA,
donald.anton@srnl.doe.gov

Abstract

It is important to understand and quantify the potential risk resulting from accidental environmental exposure of condensed phase hydrogen storage materials under differing environmental exposure scenarios. This paper describes a modeling and experimental study with the aim of predicting consequences of the accidental release of $2LiBH_4+MgH_2$ from hydrogen storage systems. The methodology and results developed in this work are directly applicable to any solid hydride material and/or accident scenario using appropriate boundary conditions and empirical data.

The ability to predict hydride behavior for hypothesized accident scenerios facilitates an assessment of the of risk associated with the utilization of a particular hydride. To this end, an idealized finite volume model was developed to represent the behavior of dispersed hydride from a breached system. Semi-empirical thermodynamic calculations and substantiating calorimetric experiments were performed in order to quantify the energy released, energy release rates and to quantify the reaction products resulting from water and air exposure of a lithium borohydride and magnesium hydride combination.

The hydrides, $LiBH_4$ and MgH_2, were studied individually in the as-received form and in the 2:1 "destabilized" mixture. Liquid water hydrolysis reactions were performed in a Calvet calorimeter equipped with a mixing cell using neutral water. Water vapor and oxygen gas phase reactivity measurements were performed at varying relative humidities and temperatures by modifying the calorimeter and utilizing a gas circulating flow cell apparatus. The results of these calorimetric measurements were compared with standardized United Nations (UN) based test results for air and water reactivity and used to develop quantitative kinetic expressions for hydrolysis and air oxidation in these systems. Thermodynamic parameters obtained from these tests were then inputted into a computational fluid dynamics model to predict both the hydrogen generation rates and concentrations along with localized temperature distributions. The results of these numerical simulations can be used to predict ignition events and the resultant conclusions will be discussed.

Introduction

Extensive studies on the safe handeling and properties of hydrogen gas released in air have been published [1]. The most important risks having been investigated were associated with possible hydrogen gas release, ignition, combustion, and/or possible detonation. Even though these risks have been evaluated, there is much less understood about the impact of air and water oxidation on solid state hydrogen storage materials, which will need to be implimented. One of the leading hydride system is "destablized" $2LiBH_4:MgH_2$. The "destabilized" mixture has been reported to have a >10 wt% H_2 capacity and rechargeable under reasonable pressure and temperature (1 to 10 atm and 20 to 100^oC) [2-3]. Environmental exposure studies of storage materials are needed to quantify the reaction pathway, products and the quantity of heat released after a possible storage tank rupture or release scenarios. For example, the hydrolysis of lithium borohydride reacts with water as follows:

$$LiBH_4 + 2H_2O(l) \rightarrow LiBO_2 + 4H_2(g) \qquad (1)$$

The hydrogen producing reaction, Equation 1, is an exothermic reaction with an enthalpy of 390 kJ/mol. The heat released from this reaction may be combined with the released hydrogen and, along with oxygen present in the surrounding air, could provide the necessary conditions for ignition. The risks of this occuring depend on the reactivity of the material, the heat liberated through reaction, the concentration of the reactants and their spatial distribution, the material packing, ambient conditions, and associated heat transfer characteristics. Therefore, this report will (i) use calorimetric techniques to quantify the heat of generation during environmental exposure scenarios for $2LiBH_4:MgH_2$ and (ii) use a simplified numerical model to predict the release and risks of hydrogen ignition under different environment scenarios.

Procedure

Experimental

Hydrolysis and oxidation studies were performed in a Calvet calorimeter equipped with a mixing cell using (deionized or distilled) water to react 5-10 mg of solid with 1 ml of liquid. Gas phase reactivity measurements were conducted to examine the oxidation and gas phase hydrolysis at varying relative humidity levels (30 and 60% RH) and temperatures (40 and 70 ^oC). For these measurements, the calorimeter equipped with a flow cell utlilizing either argon or air as the carrier gas with a flow rate of 10 ml/min reacting with 5-10 mg of solid. Table 1 outlines the test matrix.

Table 1: Experimental Test Matrix

Condition /Carrier Gas	**Mixing (neutral water)**	**Dry**	**RH Flow**	
			30%	**60%**
Argon	×	×	×	×
Air	×	×	×	×

Numerical Modeling

The numerical simulation examined an aggrigation of storage material in four different accident scenerios. In each scenario, the hydride has been released from its containment vessel and formed an axisymmetric heap, making a two-dimensional axisymmetric model appropriate. The governing equations solved for each analysis include mass, momentum, and energy balances. FLUENT, a general purpose computational fluid dynamics (CFD) package, was used to solve the equations using the finite volume approximation method [4]. Figure 1 provides the grid geometry with accompanying dimensions, while Table 2 lists the model parameters used based on Hardy, 2007 [5]. The grid consists of 26,700 elements (26,400 nodes) created using a fixed sizing function where the grid size ranges from 0.25 mm (along the material pile boundary) to 2.5 mm (within the ambient) with growth rate of 1.02.

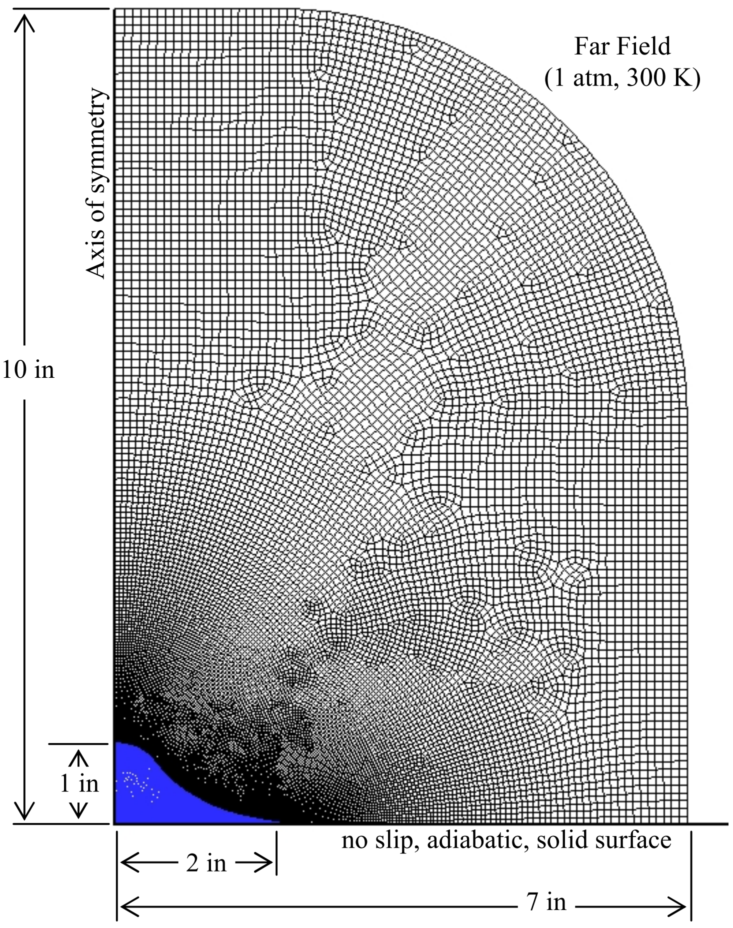

Figure 1 Axisymmetric Grid with Model Dimensions.

Table 2 Model Parameters for Porous $NaAlH_4$ [5]

Parameter	Value
Material porosity (ε)	0.5
Particle Diameter (D_p)	3.7×10^{-6} m
Material density (ρ)	720 kg/m^3
Material thermal conductivity (k)	0.325 W/m-K
Material specific heat (C_p)	820 J/kg-K
Heat generation	≤ 40,000 J/mol (overall heat of reaction for $NaAlH_4$ from NaH)
Mass generation	≤ 0.5 kg H_2/m^3-s (loading based on DOE 2010 Technical Target)

The four accident scenarios considered here are described in Table 3. In each scenario, a pile of hydrogen storage material in an arbitrary form is exposed to the ambient air, resulting in a chemical reaction that releases hydrogen and heat. However, the location and magnitude of the generation source is different for each scenario. The source locations are provided in Figure 7. These source locations correspond to hydride falling on a dry surface on a dry day, a wet surface on a dry day, a wet surface on a rainy day and a dry surface on a rainy day. The heat generation is based arbitrarily on the overall heat of reaction for the production of $NaAlH_4$ forming from NaH, while the hydrogen mass generation is based loosely on material meeting the DOE 2010 Technical Targets for hydrogen storage [5].

The following assumptions were made to simplify the analysis. In general, all constants not derived from experimental data will be replaced by experimentally verified data or correlations in future work.

- The ambient is fluid in dry air for all simulations. Water vapor is not modeled, even when the ambient is "30% RH air".
- Chemical reactions are not modeled within the pile of material or the ambient fluid. The effects of the chemical reactions within the pile of material are represented by heat and mass generation sources.
- The heat and mass generation sources remain constant throughout each scenario.
- The material is a uniform porous media throughout the pile, both within the source area and the remainder of the pile.
- The material properties do not change during the simulation.
- The ambient air properties are allowed to change with the ideal gas law.

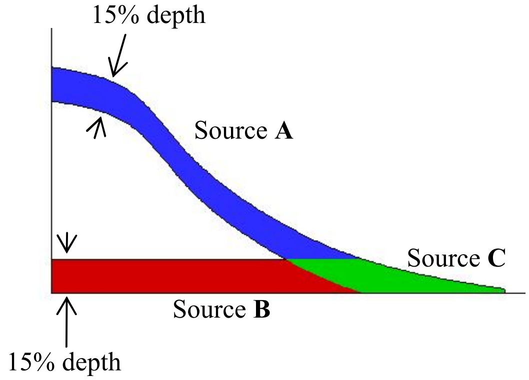

Figure 7 Schematic of Sources for the Model Accident Scenarios.

Table 3 Model Accident Scenarios

Scenario	Description	Generation**	Schematic
1. Bottom only source	Pile of material on a wet surface in dry air*	Sources **B** and **C**: Heat Generation = 40,000 J/mol Mass Generation = 0.5 kg H_2/m^3-s	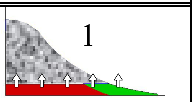
2. Top only source	Pile of material on a dry surface with the pile exposed to 30% RH air*	Sources **A** and **C**: Heat Generation = 12,000 J/mol Mass Generation = 0.15 kg H_2/m^3-s	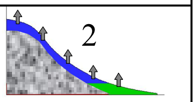
3. Dual sources with reduced top	Pile of material on a wet surface with the pile exposed to 30% RH air*	Source **A**: Heat Generation = 12,000 J/mol Mass Generation = 0.15 kg H_2/m^3-s Sources **B** and **C**: Heat Generation = 40,000 J/mol Mass Generation = 0.5 kg H_2/m^3-s	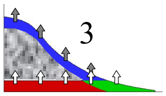
4. Dual sources with full top	Pile of material on a wet surface in the rain*	Sources **A**, **B**, and **C**: Heat Generation = 40,000 J/mol Mass Generation = 0.5 kg H_2/m^3-s	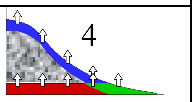

Note: * All models use dry air as the ambient. Water vapor is **not** modeled.
** Heat and mass generation sources remain **constant** through the simulations.

Results and Discussion

Hydrolysis of Charged Material

Figure 2a gives a typical calorimetric result of heat flow vs. time for liquid water hydrolysis of $2LiBH_4+MgH_2$ at 40 and 70°C. As displayed here, a specimen temperature increase of 30°C (from 40 to 70°C) resulted. The total heat released for the hydrolysis reaction was different for the two temperatures, as well as the final crystalline phase products showing somewhat different reactions occurred. Amorphous lithium products were observed at the lower 40°C temperature along with $Mg(OH)_2$, while crystalline lithium compounds such as $Li(H_2O)_4B(OH)_4(H_2O)_2$ were observed in the higher temperature hydrolysis reaction at 70°C. The integrated area under the heat flow signal at in Figure 2(a) divided by the total reaction enthalpy (total area under the heat flow signal) was used to estimate the reaction progress (in percent) as displayed in Figure 2(b). The result allows us to quantify the increase in reaction rate: a temperature increase of 30°C (from 40 to 70°C) resulted in an increase of the reaction progress from 40 to 70% after 1 hour.

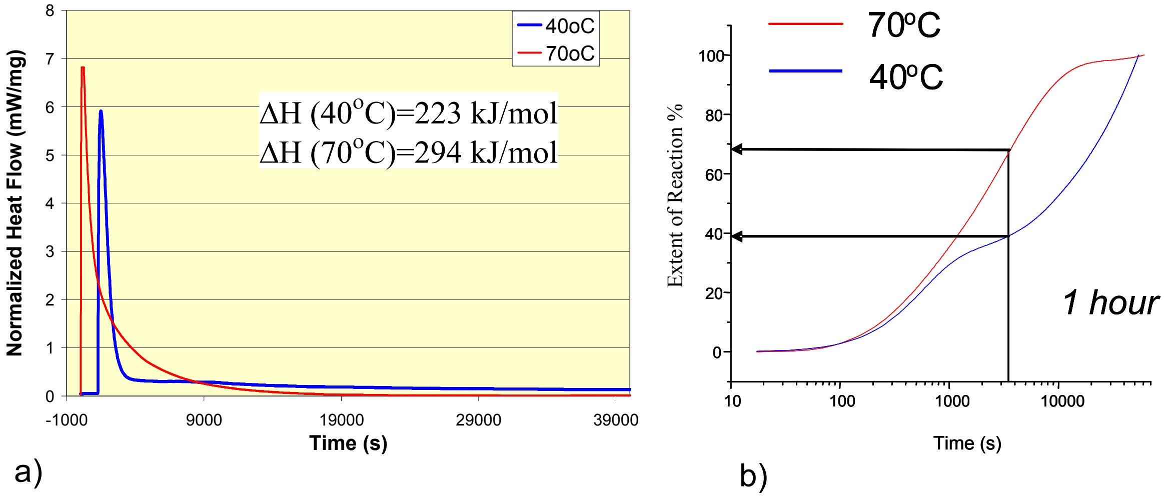

Figure 2. a) Heat flow signal from neutral water hydrolysis of $2LiBH_4$:MgH_2 at 40°C and 70°C and b) the reaction progress as a function of time determined from the integrated calorimetric signal.

Hydrolysis of Discharged Material

Figure 3 displays the heat flow signal during neutral water hydrolysis of fully discharged materials at a) 40°C and b) 70°C. Although there are slight differences in the maximum peak heat flow and the reaction enthalpy, there is not the large difference in reaction progress observed in the fully hydrided starting material shown in Figure 2. XRD analysis of the hydrolysis products indicated $Mg(OH)_2$, $Mg_5(BO_3)O(OH)_5{*}2H_2O$, and $MgB_{12}O_{19}(H_2O)_5$ crystalline species.

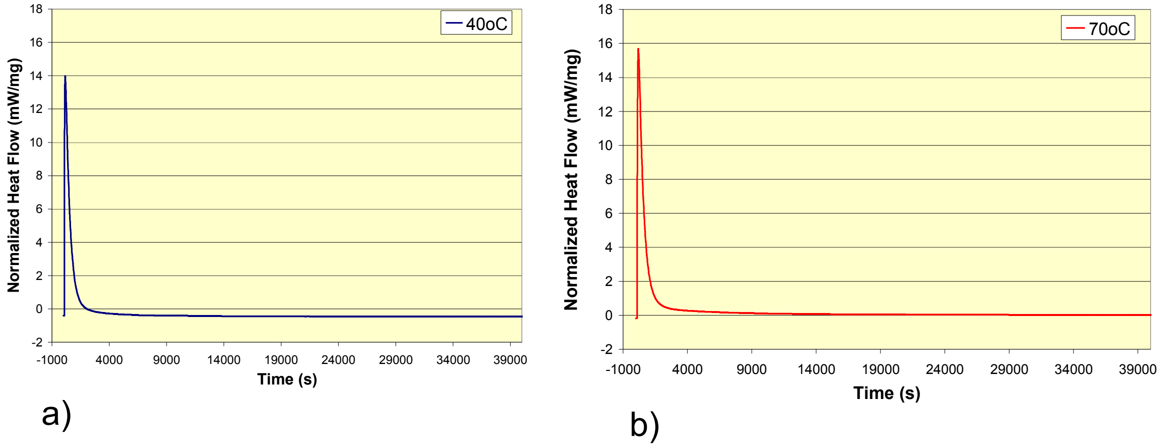

Figure 3. Heat flow signal from hydrolysis of fully discharged $2LiBH_4$:MgH_2 at a) 40°C with ΔH of 8.3 kJ/g (170 kJ/mol) b) 70°C with an enthalpy of ΔH 14 kJ/g (287 kJ/mol); kJ/mol determined using theoretical weight of 20.5 g/mol for fully discharged material.

Gas Phase Calorimetry

Air versus argon carrier gas

The effects of water vapor in air versus water vapor in an argon carrier gas were studied to separate the effects of hydrogen oxidation with air from gas phase water hydrolysis. Figure 4 displays the heat flow signal from $LiBH_4$ reacted with water vapor (30% relative humidity) at 40^{o}C using air and argon as a carrier gas flowing at 10 ml/min.

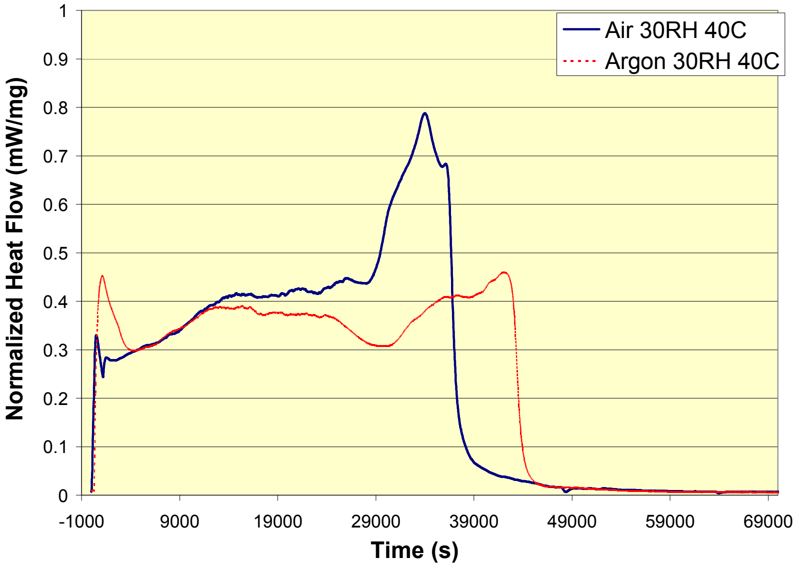

Figure 4. Normalized heat flow signal from $LiBH_4$ reacted with 30% relative humidity using air and argon as a carrier gas at 40^{o}C.

The energy release during the reaction were approximately the same for both cases: 30% RH air carrier gas 352 kJ/mol, 30% RH Argon carrier gas 340 kJ/mol, however the reaction in the presence of air reaches completion more quickly than in the presence of argon. XRD identified products were: air carrier gas ($LiB(OH)_4$, $LiB(OH)_2(O_2)$, $H_6B_2O_6$ and residual $LiBH_4$); argon carrier gas ($LiB(OH)_4$) illustrating different reactions occurred in the presence of oxygen.

Relative Humidity Effects

The heat flow signal was measured during humid air exposure for the mixture $2LiBH_4$:MgH_2 at 40^{o}C with both 30% RH and 60%RH. Figure 5 displays the multiple heat releasing events that were observed in these experiments indicating "spallation" type reactions under gas phase hydrolysis. The total amount of heat released was approximately the same at different relative humidity levels, with a value of 268 kJ/mol at 40^{o}C 30%RH and 251 kJ/mol at 40^{o}C 60%RH. The XRD results for crystalline products are displayed in Figure 6 showing $LiB(OH)_4$ and residual MgH_2 products for both levels of relative humidity. In gas phase hydrolysis, the amount of water vapor seems only to impact the reaction time and not the pathway or final products. An increase in water vapor available for hydrolysis decreases the time required to complete the reaction.

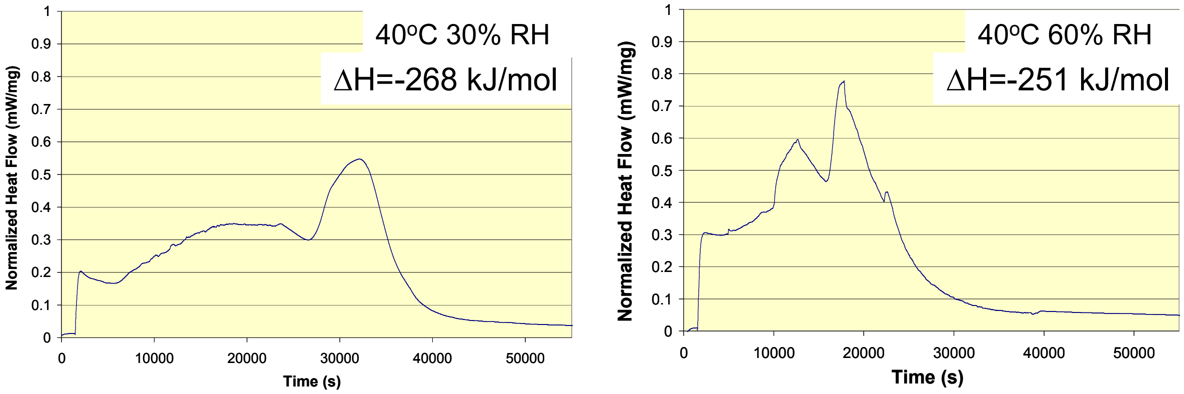

Figure 5. Normalized heat flow (mW/mg) for $2LiBH_4$:MgH_2 reacted with a) air at 40°C and 30% relative humidity and b) air at 40°C and 60% relative humidity.

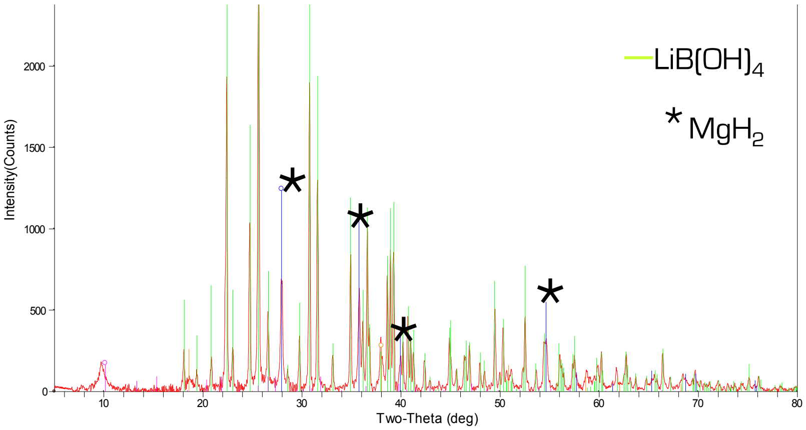

Figure 6. XRD spectrum of gas phase hydrolysis product from figure 4a.

Temperature Effects of Gas Phase Hydrolysis

The reaction of $2LiBH_4$:MgH_2 with air at 70°C and 30% relative humidity were performed, resulting in approximately the same crystalline products ($LiB(OH)_4$, and MgH_2) and total heat release (242 kJ/mol) as the reaction at 40°C at varying relative humidity levels. The only impact of increased temperature seems to be an increase in the amount of water vapor in the air, thus speeding up the hydrolysis reaction.

Numerical Modeling Results

For hydrogen ignition, the most important parameters are the flammability and explosive limits. The lower and upper flammability limits (LFL and UFL) are 4% and 75% mol fraction, respectively. The lower and upper explosive limits (LEL and UEL) are 17% and 56% mol fraction, respectively. Another important limit is the auto ignition temperature for hydrogen, which, depending on the concentration, ranges from 500°C to 571°C. Note that each simulation was initialized at 27°C with 0.00% mol fraction of H_2.

Figure 8 presents contour plots of the hydrogen concentration for each scenario after one second. Note that the flammability and explosive limits are marked with solid black lines and that each scenario is marked with a small schematic. The lower flammability (LFL, 4%) and lower explosive (LEL, 17%) limits are reached in less than one second for each scenario given the constant heat and mass generation sources. In addition, within the pile of material, the upper flammability (UFL, 75%) and upper explosive

(UEL, 56%) limits are reached in less than one second for Scenarios 1, 3, and 4. The concentration for Scenario 2, which has a top only source at 30% of the maximum generation rate, stays below 35% mol fraction after one second.

After 120 seconds of constant generation, the H_2 concentrations are lower within the storage material for each scenario compared with the concentrations after only one second, as shown by comparing Figure 9 with 8, respectively. For example, in Scenario 1, the maximum concentration is 0.93 after one second but only 0.89 after 120 seconds. This result can be attributed to the porous material generating the hydrogen, which does not allow the hydrogen to dissipate as easily as the ambient fluid and, thus, initially causes local accumulation. As the reaction continues (e.g. 120 seconds), circulation regions form in the ambient allowing for an ingress of air into the storage media that reduces the concentration of hydrogen. In addition, the top only generation source (Scenario 2) allows the hydrogen to dissipate quickly into the ambient fluid, which reduces pooling and keeps the concentration low.

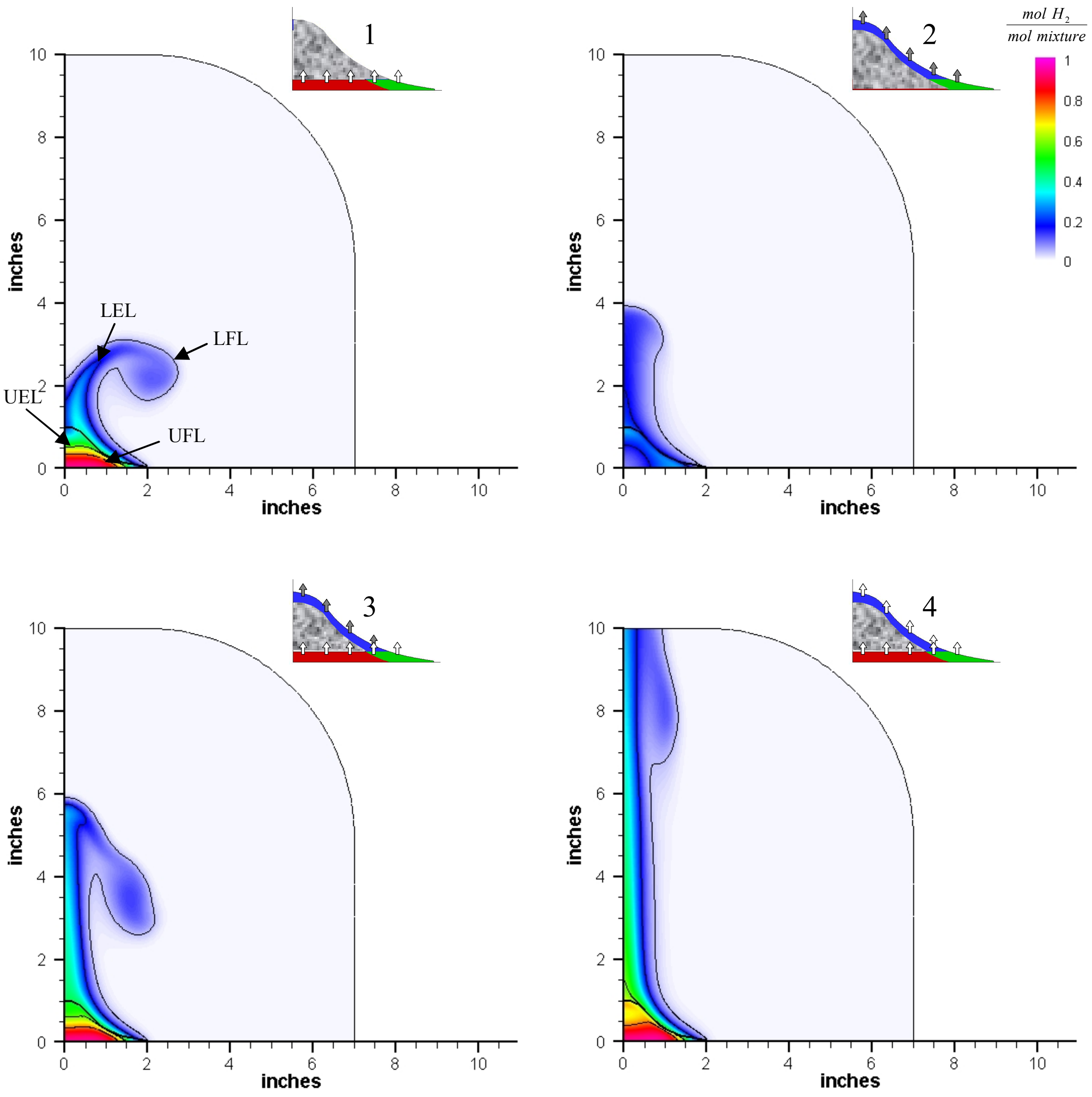

Figure 8. H_2 generation for each scenario after 1 second.

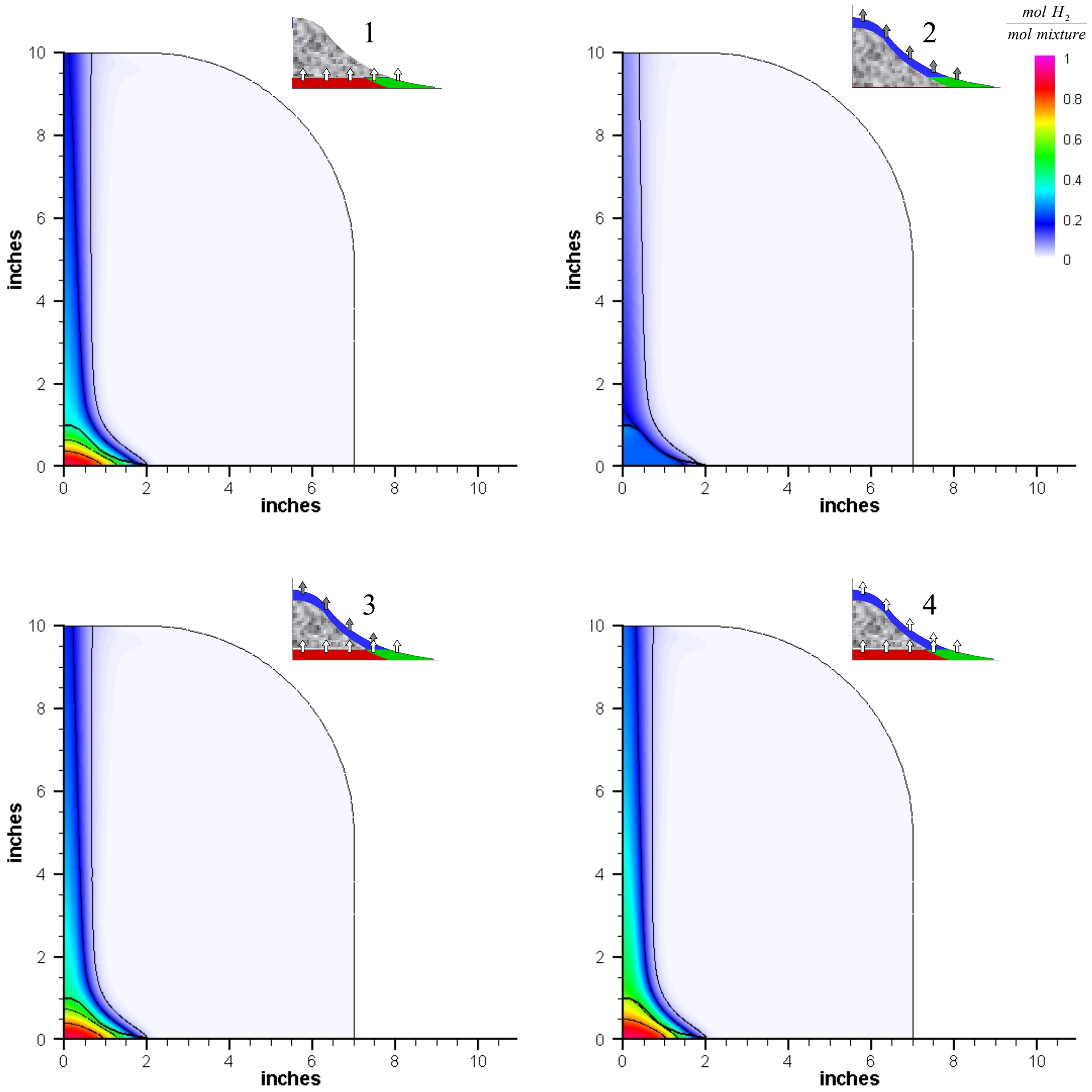

Figure 9. H_2 generation for each scenario after 120 second.

The temperature profiles for each scenario after one second are shown in Figure 10. Those scenarios with bottom generation (Scenarios 1, 3, and 4) sustain heat generation within the pile of material. Conversely, the top only generation case (Scenario 2) promotes heat dissipation from the material to the ambient.

Figure 11 presents the temperature profiles for each scenario after 120 seconds. Note that, because the heat generation is constant, the temperature will rise until thermal equilibrium is established. The bounds of the auto ignition temperature range (500°C to 571°C, depending upon the conditions) for H_2 are marked with solid black lines within the temperature profiles. Those accident scenarios with bottom generation (Scenarios 1, 3, and 4) reach the auto ignition temperature within the hydrogen storage material before 120 seconds. Table 4 provides the approximate times at which the auto ignition range bounds are reached. Scenario 4, which has maximum generation from both the top and bottom sources, is the only case to reach the auto ignition temperature within the ambient fluid above the material pile. Conversely, the top only generation source case (Scenario 2) is the only accident scenario that does not reach the auto ignition temperature after 120 seconds.

Table 4. Time to Reach the Auto Ignition Temperature

Scenario	500°C	571°C
1. Bottom only source	42 seconds	53 seconds
2. Top only source	n/a	n/a
3. Dual sources with reduced top	41 seconds	51 seconds
4. Dual sources with full top	37 seconds (65 seconds in ambient)	45 seconds (82 seconds in ambient)

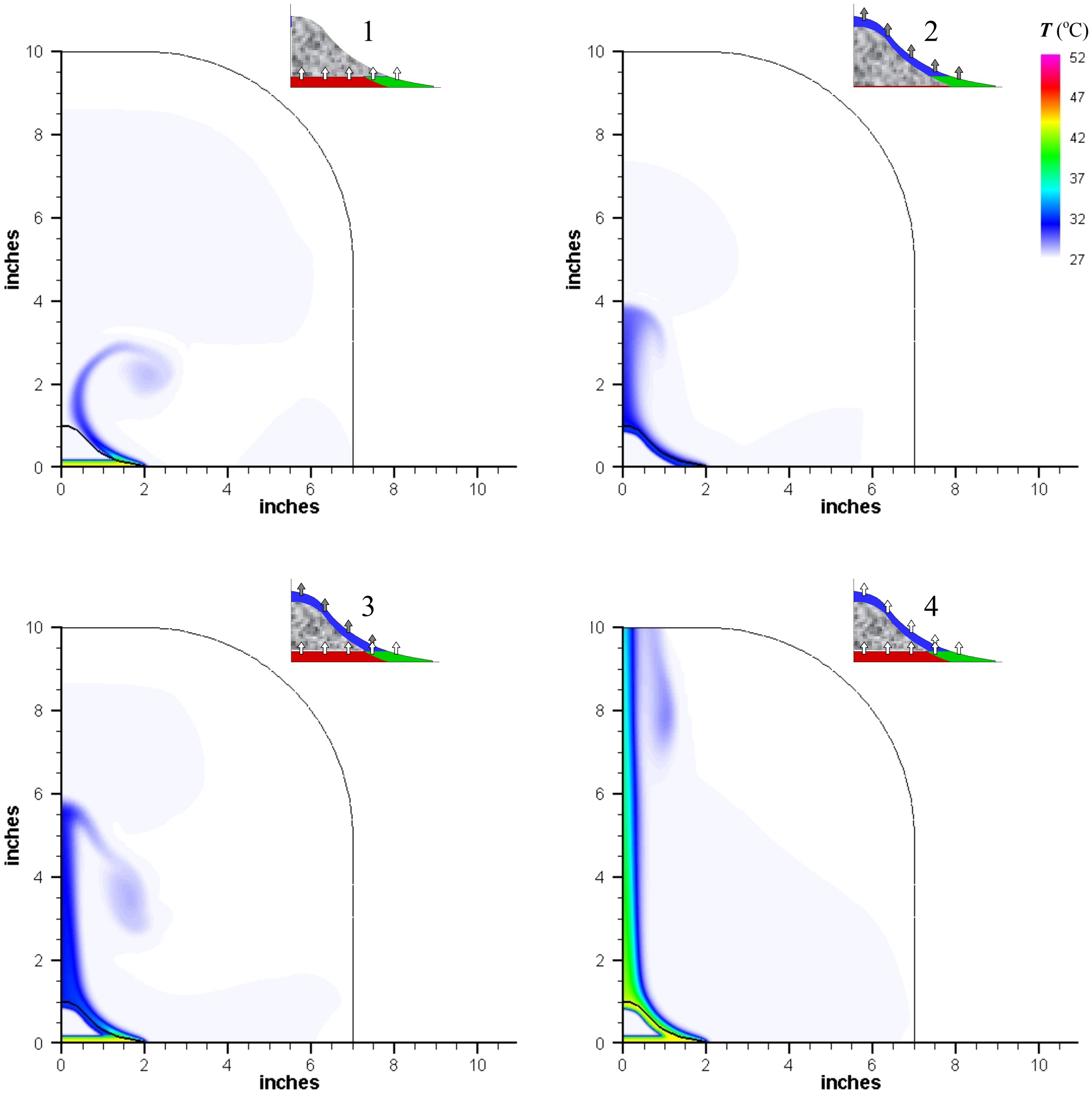

Figure 10. Temperature profiles for each scenario after 1.0 seconds.

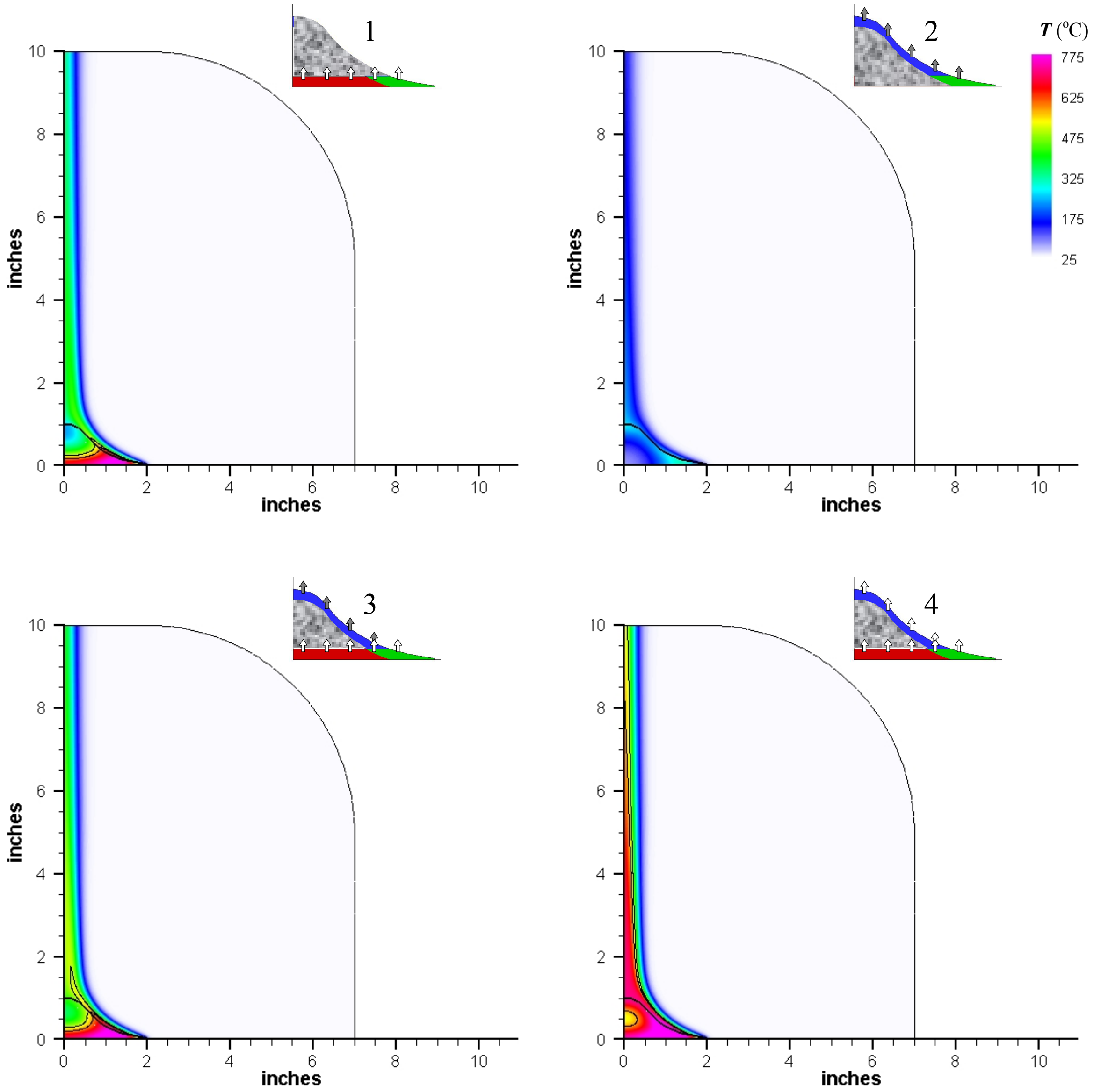

Figure 11. Temperature profiles for each scenario after 120 seconds.

The preceding modeling results represent the initial steps in an ongoing effort that will attempt to model accident scenarios for hydrogen storage materials. The goal of this phase was to model multiple species with a porous media and heat and mass generation sources. This model was a simplified representation that used constant sources and general fluid and material properties. During the next phase of analysis, experimental data, i.e.-calorimetry, will be used to tailor these simplified models to be more representative of the complex chemical reactions present in these accident scenarios.

Conclusions

The heat flow of destabilized $2LiBH_4$:MgH_2 system was measured under different conditions that simulated various environmental conditions (dry, humid, and wet). The total heat released and the final crystalline products were different for the hydrolysis reaction at 40°C and 70°C. Amorphous lithium products were observed at the lower 40°C temperature, while crystalline lithium compounds were observed at 70°C. In the gas phase reaction, the presence of water vapor increased the reaction time, but does not change the final product. For the numerical modeling, Scenario 4, which has maximum generation from both the top and bottom sources, is the only case to reach the auto ignition temperature within the ambient fluid above the material pile. Conversely, Scenario 2, which only has a generation source located at the top of the pile of material, is the only accident scenario that does not reach the auto ignition temperature after 120 seconds.

References

1. Fischer, M., Safety Aspects of Hydrogen Combustion in Hydrogen Energy-Systems. *International Journal of Hydrogen Engery*, **11**, No. 9, 1986, pp 593-601.
2. Satyapal, S., et al., The US Department of Energy's National Hydrogen Storage Project: Progress towards meeting hydrogen-powered vehicle requirements. *Catalysis Today*, **120**, No. 3-4, 2007, pp 246-256.
3. Vajo, J.J. and G.L. Olson, Hydrogen Storage in Destabilized Chemical Systems, *Scripta Materialia*, **56**, No. 10, 2007, pp 829-834.
4. FLUENT6, Fluent, Inc., 2005.
5. Hardy, B.J., Integrated Hydrogen Storage System Model. *Report, WSRC-TR-2007-00440, rev. 0*. Savannah River National Laboratory. Available from: http://sti.srs.gov/fulltext/WSRC-TR-s002-00440.pdf. November 16, 2007.